# Determination of Exciton-Phonon Coupling Elements in Single-Walled Carbon Nanotubes by Raman Overtone Analysis

Andrew P. Shreve,[1] Erik H. Haroz,[1] Sergei M. Bachilo,[2] R. Bruce Weisman,[2] Sergei Tretiak,[1] Svetlana Kilina,[1] and Stephen K. Doorn[1,*]

[1]*Los Alamos National Laboratory, Los Alamos, New Mexico 87545, USA*

[2]*Department of Chemistry, Rice University, 6100 Main Street, Houston, Texas 77005, USA*

(Received 20 July 2006; published 19 January 2007)

Raman excitation profiles are obtained and compared for carbon nanotube radial breathing mode (RBM) fundamental and overtone vibrations for 5 specific chiralities. Fitting of the Raman excitation data is performed using Raman transform theory. The Huang-Rhys factors obtained from the modeling are directly related to the magnitude of the RBM exciton-phonon coupling element, which is shown to be in a weak coupling limit. The values of exciton-phonon coupling strengths and the possible role of revealed non-Condon effects are in agreement with quantum-chemical modeling.

DOI: 10.1103/PhysRevLett.98.037405 PACS numbers: 78.67.Ch, 63.20.Ls, 63.22.+m, 78.30.−j

Carbon nanotubes are important low-dimensional materials with a variety of physical behaviors, of both fundamental and applied interest, in which electron-phonon coupling can play a significant role. High electron mobility in carbon nanotubes is one feature that makes them attractive for nanoscale electronics applications. More recently, with the demonstration of light emission from semiconducting nanotubes [1], photonic and electro-optic applications [2,3] have been envisioned. Both transport and optical phenomena are impacted by the magnitude of electron-phonon and exciton-phonon coupling. Phonon scattering results in significant loss in mobility at high applied fields in nanotube electronic devices [4]. Phonon-assisted absorbance features observed in photoluminescence excitation spectra [5,6], and phonon sidebands observed in photoconductivity spectra [7] demonstrate the importance of exciton-phonon coupling for optical processes in nanotubes. A number of theoretical efforts have recently appeared to describe these results [8,9]. Pronounced chirality dependent effects on nanotube radial breathing mode (RBM) Raman scattering intensities have also recently been observed [10–12], and shown to arise from chirality dependences appearing in the exciton-phonon coupling matrix element [13–16].

Nanotubes have been considered to be weakly exciton-phonon-coupled systems in the past, but recent photoluminescence excitation (PLE) and photoconductivity results suggest that this may not be the case [5–7,17]. However, there have been no direct quantitative measurements of the magnitude of exciton-phonon coupling, and these recent studies were focused instead on the unexpected observation and description of phonon-assisted processes as an indication of the importance of the coupling in nanotubes. Thus, there exists a need for quantitative experimental determination of exciton-phonon coupling strength.

The ratio of Raman fundamental to overtone intensities depends upon exciton-phonon coupling strength [18,19]. In this Letter we fit Raman excitation profiles for RBM fundamental and overtones for several nanotube chiralities, using Raman transform theory [19–22]. This modeling yields the Huang-Rhys factor ($S$), which is commonly used to characterize linear vibrational coupling to electronic excitations through the difference between ground and excited state geometries. The Huang-Rhys factor can be related to the displacement between the minimum energy positions of harmonic vibrational potentials associated with ground and excited electronic states by the expression

$$S = \Delta^2/2, \tag{1}$$

where $\Delta$ is a dimensionless displacement expressed in units of $\sqrt{\hbar/\mu\omega}$, with $\mu$ being the reduced mass of the vibrational coordinate. For comparison with exciton-phonon coupling models other than displaced harmonic oscillators, the Huang-Rhys factor is related to an exciton-phonon coupling element $V_{\mathrm{ep}}$, defined here as the gradient (in dimensionless coordinates) of the electronic transition energy along the vibrational coordinate of interest, as

$$S = (1/2)(V_{\mathrm{ep}}/\hbar\omega)^2, \tag{2}$$

where $\omega$ is the frequency of the given vibration (here the RBM).

In molecular spectroscopy, Franck-Condon overlap factors, related to $S$, determine the probability of specific electronic-vibrational transitions that give rise to vibrational replicas in absorption and fluorescence spectra. Subsequently, $S$ characterizes the strength of exciton-vibration coupling, with values of $S \leq 0.1$ interpreted as weak exciton-vibration coupling. In the current work, we determine Huang-Rhys factors for the second excitonic transition ($E_{22}$) in 5 different nanotube chiralities belonging to the $\nu = (n - m)\mathrm{mod}3 = -1$ (referred to as ''mod2'') group using fitting of experimental Raman profiles and also provide comparison to quantum-chemical

 

calculations. Exciton-phonon coupling for the RBM is found to be in a weak coupling regime.

Raman excitation profiles were obtained with Ti:sapphire laser excitation in the region 700 to 850 nm on HiPco-produced carbon nanotubes suspended in sodium dodecyl sulfate solution, as described previously [10]. PLE spectra were obtained from similar samples on a J-Y Spex Fluorolog 3–211 (see Ref. [23]). An example of Raman spectra for the RBM region is shown in Fig. 1. Overtone spectra are significantly weaker than the fundamental, with frequencies almost exactly twice that of the fundamentals, indicating low anharmonicity. Nanotubes described by a specific $(n, m)$ structural index may be unambiguously identified, and spectrally isolated, due to the known variation of RBM frequencies and transition energies with $(n, m)$ [10,11,23]. Individual Raman spectra were deconvoluted using Lorentzian peak fitting of the RBM fundamental and overtone features. Peak intensities from the deconvoluted spectra, referenced against an external standard corrected for the $\omega^4$ excitation frequency prefactor for nonresonant Raman scattering, were then used to generate chirality specific excitation profiles shown in Fig. 2. In general, the ability to obtain high quality profiles for both the fundamental and overtone was limited by the level of noise present in the weak overtone region, but profiles suitable for our modeling approach were obtained for 5 different chiralities.

Modeling of Raman scattering intensities under various sets of assumptions in order to obtain information on exciton-phonon coupling strengths is a well-developed field. Raman transform theory allows direct calculation of fundamental and overtone excitation profiles using, as input, a line shape function derived from the electronic absorption spectrum [19–22]. The implementation used here includes thermalization and non-Condon effects [19,22]. The latter introduce vibrational coordinate dependence into the electronic transition dipole through a power series expansion. Assumptions invoked in our modeling are (1) Raman scattering is treated at $n$th order in the time-correlator or transform theory sense (but nonperturbatively in the exciton-phonon coupling [22]), where $n = 1$ and 2 for the fundamental and overtone excitation profiles, respectively; (2) the fluorescence excitation spectrum of a particular chirality nanotube is taken to provide an accurate measure of its absorption spectrum; (3) this spectrum corresponds to a homogeneous electronic line shape in the resonance Raman sense, consistent with recent observations [24]; (4) vibrational frequencies of the RBM are equal in the ground and excited electronic states, also consistent with recent calculations [25]; and (5) the RBM is separable from all other vibrations.

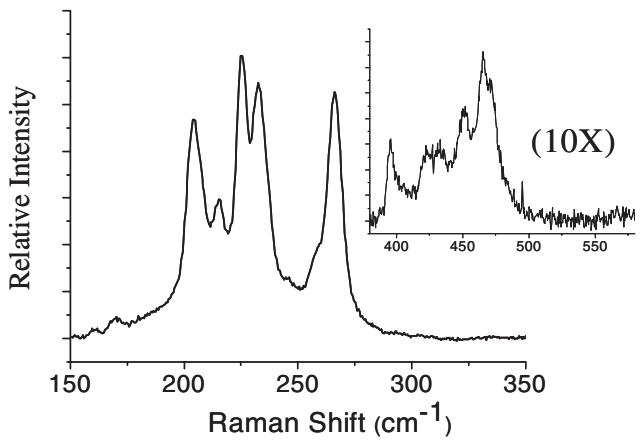


FIG. 1. Fundamental and first overtone (inset) Raman spectra of the RBM region for 766 nm excitation.

The modeling procedure is as follows. PLE spectra are manipulated by background subtraction and, if need be, truncation, to remove excitation features associated with other nanotube chiralities having nearby emission wavelengths. If necessary due to truncation, then a smooth extrapolation to the baseline is added, and finally, a smooth curve is generated using a spline interpolation method (Fig. 2). This curve is used as the absorption spectrum, $A(\omega)$, in the transform calculation.

From $A(\omega)$, the line shape function $\phi(\omega)$ is calculated as

$$\phi(\omega) = \frac{1}{\pi} P \int_{-\infty}^{+\infty} d\omega' \frac{A(\omega')}{\omega'(\omega' - \omega)} + \frac{iA(\omega)}{\omega}, \quad (3)$$

where a principal value integral is taken. Then, the fundamental Raman excitation profile is

$$F(\omega) = KS\omega(\omega - \omega_v)^3(\bar{n}_v + 1) \times |(1 + C)\phi(\omega) - (1 - C)\phi(\omega - \omega_v)|^2, \quad (4)$$

where $K$ is a numerical constant, $S$ is the Huang-Rhys factor, $\omega_v$ is the energy of one vibrational quantum, $\bar{n}_v$ is the average thermal occupation number for a mode of energy $\omega_v$ (calculated for $T = 295$ K in our case), and $C$ is the non-Condon parameter. Likewise, the overtone excitation profile is

$$G(\omega) = \frac{1}{2} KS^2\omega(\omega - 2\omega_v)^3(\bar{n}_v + 1)^2|(1 + 2C)\phi(\omega) - 2\phi(\omega - \omega_v) + (1 - 2C)\phi(\omega - 2\omega_v)|^2. \quad (5)$$

In practice, for small $S$ and for unstructured excitation profiles, the value of $C$ primarily affects the peak position of the Raman excitation profiles relative to the peak position of the fluorescence excitation profile, while $S$ primarily affects the magnitude of the overtone intensity relative to the fundamental intensity.

Examples of fits to data are provided in Fig. 2, with parameters given in Table I. Resultant $S$ values vary from 0.013 to 0.025, corresponding to a range of 5.1 to 7.3 meV for the exciton-phonon coupling elements [as given by Eq. (2)]. We estimate uncertainties in the values of Huang-Rhys parameters to be $\pm 20\%$, while uncertainties in the non-Condon parameter are typically $\pm 0.15$. Examples of model results obtained for a range of values of $S$ and $C$ are presented in the supplementary information in [26] for the

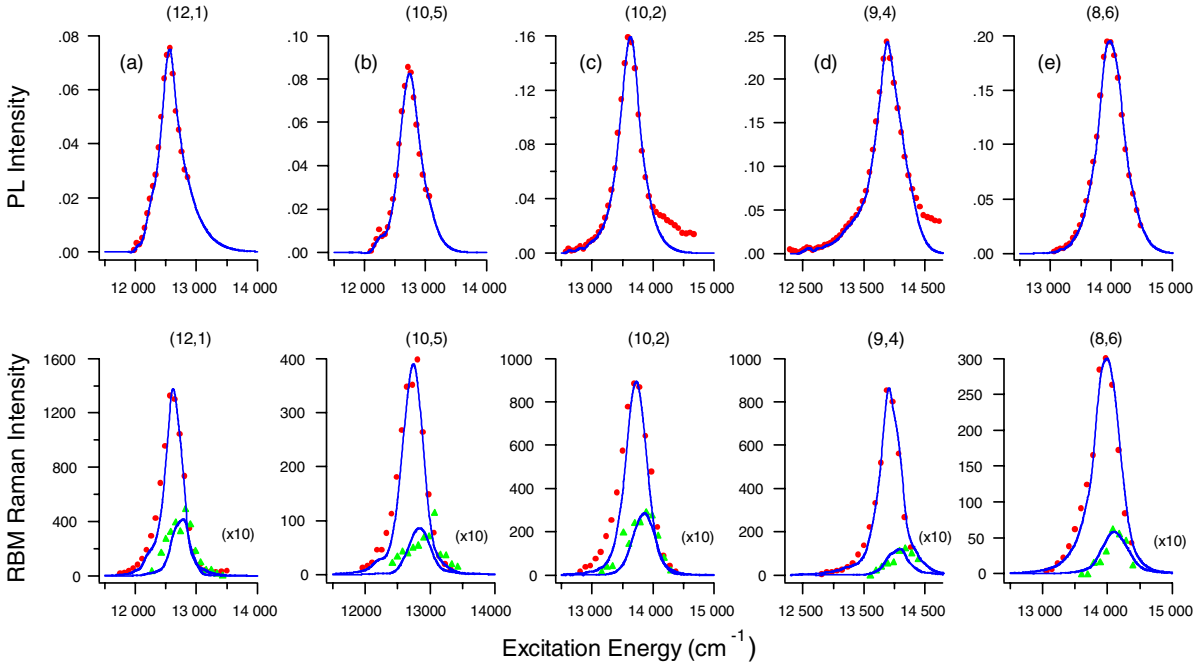


FIG. 2 (color online). Top panels show PLE spectra (points) and the functions used as input to Raman transform theory models (solid lines). Bottom panels show experimental Raman excitation profiles for the RBM fundamental (circles) and overtone (triangles), along with fits obtained using Raman transform methods and parameters presented in Table I. Raman intensities are for RBM and overtone frequencies, respectively, observed for the following chiralities at: (a) (12,1): 236 $cm^{-1}$/473 $cm^{-1}$, (b) (10,5): 226 $cm^{-1}$/452 $cm^{-1}$, (c) (10,2): 266 $cm^{-1}$/531 $cm^{-1}$, (d) (9,4): 257 $cm^{-1}$/514 $cm^{-1}$, and (e) (8,6): 245 $cm^{-1}$/489 $cm^{-1}$. Overtone intensities have been multiplied by a factor of 10 for clarity.

(8,6) chirality nanotube. The magnitude of the Huang-Rhys factors shown in Table I is consistent with the relative weakness (compared to zero-phonon features) of intensities observed for phonon sidebands and phonon-assisted absorption features, as well as with observations of small (<8 meV) Stokes shifts in nanotube spectra [5,7,17]. Significantly, this result also confirms recent modeling studies that suggest the RBM couples only weakly to transport scattering processes and electro-optic phenomena [7,8].

Our main results here are the values of the Huang-Rhys parameter. However, we also find that nonzero non-Condon parameters are required for successful modeling of the Raman excitation profiles. In the present case, non-Condon contributions primarily serve to shift the energy position of the Raman excitation profiles, so the need for such terms does depend upon our assumption that a nanotube's absorption spectrum matches its PLE spectrum. In addition, the determination of non-Condon parameters whose absolute values exceed $\approx 0.1$, observed here in some cases, formally exceeds the range of validity of the linear non-Condon approximation used in deriving Eqs. (4) and (5). Nevertheless, our analysis suggests that, within the context of molecular spectroscopy, non-Condon effects should be further explored in studies of carbon nanotube excitations. Such effects may be found in spectroscopic signatures of vibrationally mediated mixing of electronic states and potentially in combination band progressions in higher frequency modes [5].

To confirm and interpret experimental findings we further utilize quantum-chemical calculations [25,27] to de-

TABLE I. Huang-Rhys factors ($S$), displacements $\Delta$, non-Condon parameters ($C$), and vibrational frequencies ($\omega_v$) determined by or used in the transform theory calculations (exp.) with results presented in Fig. 2, and the corresponding theoretically calculated values (th.) using approximate Eq. (1) ($S_A$ and $\Delta_A$) and excited state geometry optimization ($S$ and $\Delta$).

| Chirality | $C$ | $\omega_v$, $cm^{-1}$ (exp.) | $\omega_v$, $cm^{-1}$ (th.) | $S$, $E_{22}$, (exp.) | $\Delta$, $E_{22}$, (exp.) | $S_A$, $E_{22}$, (th.) | $\Delta_A$, $E_{22}$, (th.) | $S_A$, $E_{11}$, (th.) | $\Delta_A$, $E_{11}$, (th.) | $S$, $E_{11}$, (th.) | $\Delta$, $E_{11}$, (th.) |
|---|---|---|---|---|---|---|---|---|---|---|---|
| (10,2) | 0.1 | 266 | 326 | 0.025 | 0.224 | 0.0085 | 0.130 | 0.0056 | 0.106 | 0.006 84 | 0.117 |
| (9,4) | 0.2 | 257 | 315 | 0.013 | 0.161 | 0.0105 | 0.145 | 0.006 96 | 0.118 | 0.007 56 | 0.123 |
| (8,6) | 0.4 | 245 | 298 | 0.017 | 0.190 | 0.0163 | 0.180 | 0.0123 | 0.157 | 0.012 32 | 0.157 |
| (12,1) | 0.1 | 236 | - | 0.025 | 0.224 | - | - | - | - | - | - |
| (10,5) | 0.4 | 226 | 274 | 0.017 | 0.190 | 0.0100 | 0.141 | 0.007 55 | 0.123 | 0.009 66 | 0.139 |

termine ground and excited state geometries of several nanotubes. We have computed 4 finite-size chiral tubes (10,2), (9,4), (8,6), and (10,5) with 2, 1, 3, and 6 repeat units in length, respectively. The underlying Hamiltonian (Austin Model 1, AM1 [28]) has the vibrational couplings and anharmonicity effects built into the dependence of its matrix elements on the nuclei positions. The excitonic effects are also included in the electronic structure methodology: time-dependent Hartree-Fock technique [27] used for excited state calculations. To address $E_{22}$ vibrational coupling, we calculated the gradients of the electronic transition energy for both $E_{11}$ (first excitonic transition) and $E_{22}$ along the vibrational coordinates and used Eq. (2) to estimate the Huang-Rhys factors and displacements $\Delta$ (see also [26]).

The results of the quantum-chemical calculations are summarized in Table I. Among (3N-6) vibrational coordinates, the RBM can be easily identified as having the largest Huang-Rhys factors in the low-frequency vibrational region. The computed RBM frequencies overestimate experimental values indicating "stiffer" tubes in theory, which is expected in the semiempirical methods used. Calculated $E_{11}$ displacements for the mod 2 tubes in question are slightly smaller than the previously reported value of 0.2 for the mod 1 (7,6) tube [25]. In contrast to (7,6), an exciton-phonon coupling displaces the tube geometry along the RBM coordinate leading to an average decrease of the diameter in the middle of the mod 2 systems [25]. A different trend is observed for $E_{22}$ vibrational couplings. Calculated displacements for $E_{22}$ are in general larger than the corresponding $E_{11}$ values, which is expected for the mod 2 family. Even though they underestimate the experimental values, reflecting increased tube stiffness, we observe an excellent agreement between theory and experimental fitting for all derived Huang-Rhys parameters across the entire nanotube set explored. Compared to $E_{11}$, the calculated $E_{22}$ displacements along RBM have opposite signs, in agreement with the local density functional results [14].

In conclusion, we have measured Raman excitation profiles for the fundamental and first overtone transitions of the radial breathing mode in carbon nanotubes of five different chiralities. Analysis of these data has allowed us to estimate the strength of the Huang-Rhys parameter, related to exciton-phonon coupling strength, for the RBM in these nanotubes. Values for the Huang-Rhys parameter ranging from 0.013 to 0.025 have been obtained, which places carbon nanotubes in a regime of weak exciton-phonon coupling strength. Modeling using Raman transform methods also provides evidence that non-Condon activity, typically indicative of vibrationally mediated coupling of electronic excited states, may play a role in a molecular description of electronic excitations of nanotubes. Overall, these studies also generally illustrate the use of resonance Raman fundamental and overtone spectroscopy as a means of exploring the coupling of electronic and vibrational responses in carbon nanotubes. These first quantitative, experimentally based, estimates of exciton-phonon coupling strength in carbon nanotubes will help constrain theoretical estimates of exciton-phonon coupling strengths and also help guide models of how exciton-phonon coupling influences electronic processes in these important materials.

A. P. S. and S. T. acknowledge support from the DOE Office of Science (Basic Energy Sciences). S. K. D. acknowledges support of the LANL LDRD program. S. K. and S. T. acknowledge support of the Center for Nonlinear Studies (CNLS) at LANL. S. M. B. and R. B. W. acknowledge support from the NSF (CHE-0314270).

*To whom all correspondence should be addressed. Electronic address: skdoorn@lanl.gov

[1] M. J. O'Connell *et al.*, Science **297**, 593 (2002).
[2] M. Freitag *et al.*, Nano Lett. **3**, 1067 (2003).
[3] J. A. Misewich *et al.*, Science **300**, 783 (2003).
[4] Z. Yao, C. L. Kane, and C. Dekker, Phys. Rev. Lett. **84**, 2941 (2000).
[5] H. Htoon *et al.*, Phys. Rev. Lett. **94**, 127403 (2005).
[6] S. G. Chou *et al.*, Phys. Rev. Lett. **94**, 127402 (2005).
[7] X. Qiu *et al.*, Nano Lett. **5**, 749 (2005).
[8] V. Perebeinos, J. Tersoff, and Ph. Avouris, Phys. Rev. Lett. **94**, 086802 (2005).
[9] J. Jiang *et al.*, Phys. Rev. B **71**, 045417 (2005).
[10] S. K. Doorn *et al.*, Appl. Phys. A **78**, 1147 (2004).
[11] H. Telg *et al.*, Phys. Rev. Lett. **93**, 177401 (2004).
[12] A. Jorio *et al.*, Phys. Rev. B **71**, 075401 (2005).
[13] S. V. Goupalov, Phys. Rev. B **71**, 153404 (2005).
[14] M. Machon *et al.*, Phys. Rev. B **71**, 035416 (2005).
[15] J. Jiang *et al.*, Phys. Rev. B **71**, 205420 (2005).
[16] V. N. Popov, L. Henrard, and P. Lambin, Nano Lett. **4**, 1795 (2004).
[17] M. Jones *et al.*, Phys. Rev. B **71**, 115426 (2005).
[18] M. Belhadj *et al.*, J. Phys. Chem. **94**, 2160 (1990).
[19] A. C. Albrecht *et al.*, J. Chem. Phys. **101**, 1890 (1994).
[20] P. M. Champion and A. C. Albrecht, Annu. Rev. Phys. Chem. **33**, 353 (1982).
[21] V. Hizhnyakov and I. Tehver, J. Raman Spectrosc. **19**, 383 (1988).
[22] J. B. Page, in *Topics in Applied Physics: Light Scattering in Solids VI*, edited by M. Cardona and G. Güntherodt (Springer-Verlag, New York, 1991), Vol. 68, p. 17.
[23] S. M. Bachilo *et al.*, Science **298**, 2361 (2002).
[24] B. C. Satishkumar *et al.*, Phys. Rev. B **74**, 155409 (2006).
[25] A. Gambetta *et al.*, Nature Phys. **2**, 515 (2006).
[26] See EPAPS Document No. E-PRLTAO-98-053702 for examples of how transform method modeling results vary as fitting parameters are adjusted around the values reported in the main text. The file also contains additional details on quantum-chemical calculations. For more information on EPAPS, see http://www.aip.org/pubservs/epaps.html.
[27] S. Tretiak *et al.*, Phys. Rev. Lett. **89**, 097402 (2002).
[28] M. J. S. Dewar *et al.*, J. Am. Chem. Soc. **107**, 3902 (1985).